The following publication Z. Cui, W. Ma, J. Lai, H. K. Chu and Y. Guo, "Coupled Multiple Dynamic Movement Primitives Generalization for Deformable Object Manipulation," in IEEE Robotics and Automation Letters, vol. 7, no. 2, pp. 5381-5388, April 2022 is available at https://doi.org/10.1109/LRA.2022.3156656.

This is the Pre-Published Version.

Coupled Multiple Dynamic Movement Primitives Generalization for Deformable Object Manipulation

Zhenxi Cui[1], Wanyu Ma[1], Jiewen Lai[1], Henry K. Chu[1], *Member, IEEE* and Yi Guo[2], *Senior Member, IEEE*

***Abstract*—Dynamic Movement Primitives (DMP) are widely applied in movement representation due to their ability to encode tasks using generalization properties. However, the coupled multiple DMP generalization cannot be directly solved based on the original DMP formula. Prior works provide satisfactory performance for the coupled DMP generalization in rigid object manipulation, but their extension to deformable objects may degrade due to the intrinsic uncertainty of the deformable model structure and parameters. This paper introduces an adaptive term to replace the fixed term to couple multiple DMP generalizations and model the deformable object using the classic mass-spring-damper model. Based on the modeling, the manipulation of a deformable object can be treated as a second-order system, which provides additional implementation flexibility and robustness in deformable object transportation. To validate the proposed method, we perform extensive simulations for cooperatively transporting a rope and a deformable thin film, imitating the manipulation with a semi-ellipse trajectory and M-shape trajectory. We further implement our method on a dual-arm robot platform for rope manipulation with depth visual feedback. Both simulation and experiment results demonstrate satisfactory DMP generalization, collision avoidance, and configuration preservation.**

***Index Terms*—Soft object manipulation, robot trajectory planning and control**

I. Introduction

ROBOTIC coordinated manipulations, such as dual agent folding and transportation of deformable objects, have been studied for many years. The trajectory planning and robot end-effector control are non-trivial in such applications. The manipulators' trajectories are coupled and constrained by the deformable object, patterns of which cannot be shifted or deformed. Dynamic movement primitives (DMP) have been proposed to design complex trajectories for manipulators. It is advantageous in a guaranteed trajectory convergence due to the critical damping configuration in DMP. Multiple DMPs can be governed by one canonical system, making multiple agents' manipulation control convenient to design. However, the original DMP method cannot directly tackle the cooperatively transporting of deformable objects, such as folding thin cloth or transporting a bio-thin film into a 3D structure, especially when the deformable object's pattern configuration is needed to be preserved during the manipulation. To do that, each manipulator may follow a demonstrated trajectory independently, as illustrated in Fig. 1. If the DMP trajectories are generalized in an uncoupled way, it could shift the pattern configuration of the deformable objects during transportation or manipulation, which could deform the pattern and, in the worst-case scenario, damage the object. Hence, an additional coupling term needs to be introduced into the original DMP to tackle the problem of deformable object manipulation.

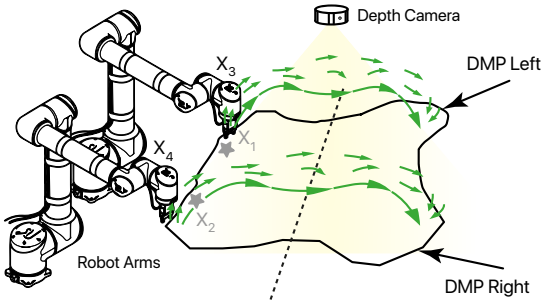

Figure 1. Coupled multipe DMP for deformable object manipulation.

A. Related Work

Multiple robot systems can transport the deformable object cooperatively by tracking the coupled DMP trajectory. Evolved from the original DMP algorithm [1], several works have been done to extend its applicability by incorporating different techniques, such as reinforcement learning [2], [3], statistical generalization [4] and the combination of obstacle avoidance algorithms [5], [6]. A temporal coupling algorithm was developed to handle velocity and acceleration constraints for solely DMP trajectories [7]. For multiple coupled DMP generalization, Kulvicius *et al.* [8] proposed a method to model the coupling term between two DMPs using a stiff virtual spring with fixed, task-specific model parameters. In this method, two robots can reach the desired position while avoiding obstacles. In [9], the velocity and acceleration of the DMP system were separately modulated by introducing a coupling term, which was iteratively updated by a learning method. It allowed the cooperative transportation of a rigid rod. Subsequently, the same group proposed to adopt adaptive stiffness control for path planning in operation space to achieve human-robot cooperation [10], [11], where speed-scaled dynamic motion primitive was applied for trajectory

Manuscript received: October 21, 2021; Revised: January 14, 2022; Accepted: February 18, 2022. This paper was recommended for publication by Editor Markus Vincze upon evaluation of the Associate Editor and Reviewers' comments. This work was supported in part by the Research Grant Council of the Hong Kong Special Administrative Region, China, under Grant 25204016. *(Corresponding author: Henry K. Chu.)*

[1]Zhenxi Cui, Wanyu Ma, Jiewen Lai, and Henry K. Chu are with the Department of Mechanical Engineering, The Hong Kong Polytechnic University, Hung Hom, Kowloon, Hong Kong 999077, China. (email: nathan.cui@connect.polyu.hk; wanyu.ma@connect.polyu.hk; jw.lai@connect.polyu.hk; henry.chu@polyu.edu.hk)

[2]Yi Guo is with the Department of Electrical and Computer Engineering, Stevens Institute of Technology, Hoboken, NJ 07030 USA. (email: yguo1@stevens.edu)

Digital Object Identifier (DOI): see top of this page.

representation, and the experiment of rigid plate transportation was conducted. In a generic DMP formulation representation, the cooperative manipulators were coupled by a coordinated transformation function [12], where a leader-follower manner was formed, and a similar final formulation result as in [9] can be achieved when only the translation term occurs in the transformation function. The effects of physical contact on the ball surface with different ball diameters and wiping manipulation were tested in simulation to validate their approach. In [13], the motion of the leader robot was observed, and the DMP parameters of the follower could be accordingly updated to complete the cooperative task. In existing works, multiple DMP coupling algorithms are applied on the rigid object scenarios of human-robot or multiple robot agents cooperative manipulation with force sensor as the feedback signal. However, multiple DMP coupled generalization based on visual feedback for deformable object manipulation has not been thoroughly investigated. In addition to the requirement of coupling multiple DMP generalization, the object model uncertainty and pattern preserving for this kind of problem can lead to extra difficulty compared to the existing works.

B. Contribution & Organization

In this paper, we focus on multiple DMP trajectory coupled generalization, which is capable of preserving the pattern configuration of the manipulated deformable object. To achieve this goal, we firstly model the deformable object by the classical mass-spring-damper model on which the multiple DMP trajectory could be dynamically coupled. Then, the multiple DMP coupled generalization and the pattern configuration preserving can be compactly integrated and simplified as a second-order system. To account for the uncertainty in the model structure and parameters of the deformable object, we employ a reference model to update the proposed coupling term adaptively. The contributions of our work are twofold:

1) We newly formulate the multiple DMP generalization and pattern preserving of the manipulated object as an integrated system, making the system modeling and control more flexible and effective.
2) Evolving from the fixed coupling term, which has been addressed in [8], [9], [11], we propose to couple the multiple DMP through the adaptive coupling term. The reference model is utilized here to dynamically modify the DMP coupling term, which would enhance the applicability of the proposed method.

This paper is organized as follows: firstly, Sec. II gives the problem statement. Next, Sec. III gives a brief review of the DMP method and introduces the proposed dynamic DMP coupling method. After that, Sec. IV and V provide necessary simulation and experiment results from different situations. Lastly, Sec. VI concludes the paper.

II. PROBLEM STATEMENT

In a dual-agent deformable object transportation problem as shown in Fig. 1, the manipulator agents, following a DMP trajectory, transport the grabbed deformable thin object from the initial position to the goal position while preserving the desired pattern (feature points) configuration. During DMP generalization, the Intel real sense 3D depth camera captured the feature points coordinates. Then, the features' norm distance would be computed and feedback to design the control coupling input for the multiple DMP generalization. As a well-known physically-based model, the mass-spring-damper model is widely used to model deformable objects, such as a rope [14] and a cloth [15] in 2D. This work also assumes that the deformable object is modeled by the mass-spring-damper model.

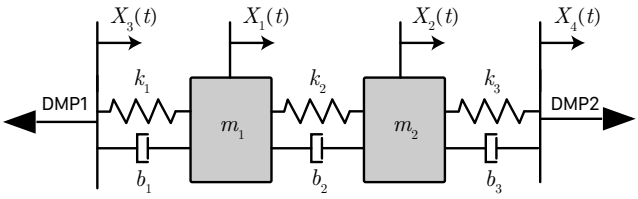

Figure 2. Model representation of the coupled system with the robot arm and features on the deformable object.

The multiple DMP trajectory generalizations can be modeled and simplified as depicted in Fig. 2 when considering only two pattern points on the object are held by two manipulator agents. Here, X_1 and $X_2 \in \mathbb{R}^3$ are the pattern points on manipulated deformable object, X_3 and $X_4 \in \mathbb{R}^3$ are the end-effector grabbing points in which the trajectory are modeled by the DMP algorithm. They are connected by the spring damper with unknown parameters k_i and b_i for $i = \{1, 2, 3\}$. To this end, the system including the manipulator's agents and pattern points can be modeled and denoted by a plant T, and the system output is the Euclidean norm between pattern points X_1 and X_2 denoted by $X_p = \|X_1 - X_2\|$, which is defined as the pattern configuration. The DMP trajectory X_3 and X_4 should be coupled by control term G, so as the system output X_p can track to the reference signal r. Without losing generality, a 2-DOF mass-spring-damper moves in a one-dimensional case to illustrate the proposed method, as illustrated in Fig. 2.

The generic state-space model of the integrated system T can be described by

$$\dot{X}_p = A_p X_p + B_p G, \tag{1}$$

where $X_p \in \mathbb{R}^n$, $G \in \mathbb{R}^m$, $A_p \in \mathbb{R}^{n\times n}$, and $B_p \in \mathbb{R}^{n\times m}$. Let us select the reference model as

$$\dot{X}_m = A_m X_m + B_m r, \tag{2}$$

where the dimensions are given as $X_m \in \mathbb{R}^n$, $A_m \in \mathbb{R}^{n\times n}$, $B_m \in \mathbb{R}^{n\times m}$, and $r \in \mathbb{R}^m$ is the reference input signal. A_m and B_m are constant-coefficient matrices. Here, the reference model is selected as

$$A_m = \begin{bmatrix} -8 & -10 \\ 1 & 0 \end{bmatrix}, \quad B_m = \begin{bmatrix} 1 \\ 0 \end{bmatrix} \tag{3}$$

to make the reference model and the plant model in the same order. To drive the output error e which is defined as $e = X_p - X_m$ asymptotically converge to 0 or $e(t)$ (depending on the system design requirements), the plant control input G in Eq. (1) should be carefully designed in the form of

$$G = h(X_p, X_m, e, r), \tag{4}$$

where h is the control input mapping function. Also, because of the uncertainty of the deformable object model structure and parameters (e.g., the unknown parameters k_i and b_i), the designed coupling term in Eq. (4) should be adaptively updated during the manipulation.

III. PROPOSED APPROACH

A. DMP Preliminary

A generic d-dimensional DMP trajectory can be modeled by a second-order ordinary differential system, which satisfies the critical damping condition of

$$\begin{aligned} \tau\dot{\nu} &= \alpha\left(\beta\left(g-x\right)-\nu\right)+f\left(q\right) \\ \tau\dot{x} &= \nu \end{aligned} \tag{5}$$

where $g \in \mathbb{R}^d$, $x \in \mathbb{R}^d$, and $\nu \in \mathbb{R}^d$ denote the goal position, current position, and velocity of the system, respectively. To avoid overshooting or slow convergence to the goal position, system parameter α and β should satisfy the relationship $\alpha = 2\sqrt{\alpha\beta}$, which leads to $\beta = \frac{\alpha}{4}$. The scalar term τ represents the temporal factor that can modulate solution evolution speed.

The vector-valued function $f : \mathbb{R} \rightarrow \mathbb{R}^d$ is the added nonlinear term in the differential equations system, which can be learned from the demonstrated trajectory. To eliminate the direct dependence on time t, function f is changed into a function of parameter q, which is governed by the canonical system:

$$\tau\dot{q} = -\alpha_c q, \tag{6}$$

where $\alpha_c > 0$. The force term $f_i\left(q\right)$, where $i = \{1, 2, \cdots, d\}$ can be formulated as

$$f_i = \frac{q\sum_j^N w_j\varphi_j\left(q\right)}{\sum_j^N \varphi_j\left(q\right)} \tag{7}$$

where $\varphi_j\left(q\right)$, with $j = \{1, 2, \cdots, N\}$, is the radial basis function, and N is the number of the basis function. More conprehensive introduction of DMP can be found in [16], [17].

B. Coupled Multiple DMP Generalization

After the Laplace transformation, the system illustrated in Fig. 2 can be modeled as

$$\begin{aligned} X_1 s^2 m_1 =& \left(-b_1 s - b_2 s - k_1 - k_2\right) X_1 \\ &+ \left(b_2 s + k_2\right) X_2 + \left(b_1 s + k_1\right) X_3 \end{aligned} \tag{8a}$$

$$\begin{aligned} X_2 s^2 m_2 =& \left(b_2 s + k_2\right) X_1 + \left(-b_2 s - b_3 s\right. \\ &\left. -k_2 - k_3\right) X_2 + \left(b_3 s + k_3\right) X_4 \end{aligned} \tag{8b}$$

$$X_3 s^2 \tau^2 = \left(-\alpha s\tau - \alpha\beta\right) X_3 + \frac{\alpha\beta g_1 + G + f_1 + O_1}{s} \tag{8c}$$

$$X_4 s^2 \tau^2 = \left(-\alpha s\tau - \alpha\beta\right) X_4 + \frac{\alpha\beta g_2 - G + f_2 + O_2}{s} \tag{8d}$$

Here, we assume that (i) $m_i = m$, (ii) $k_i = k$, and (iii) $b_i = b$, where $i \in \{1, 2, 3\}$. This condition is quite mild because of the relatively slow manipulation and the materials that preserve uniformly continuous properties in small vicinity areas. $O_i, i \in \{1, 2\}$ is the obstacle avoidance term given by

$$O_i = -\nabla_x U\left(x\right), \quad \text{where} \quad U\left(x\right) = \frac{Ae^{-\eta C(x)}}{C(x)}, \tag{9}$$

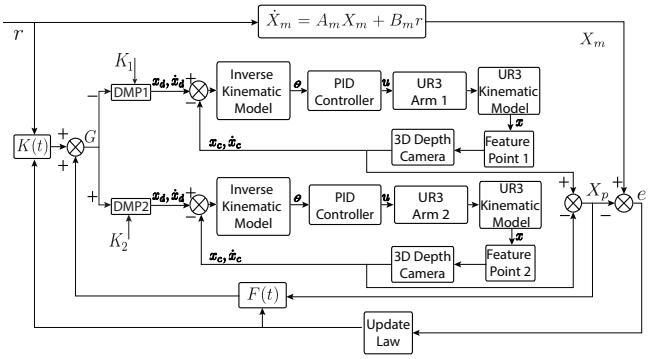

Figure 3. Control diagram of coupled DMP manipulation.

with A and η being the positive empirical parameters and $C(x)$ being an *isopotential function* [5]. By simplifying Eqs. (8a) to (8d), one can derive the system output X_p as

$$X_p = \frac{\left(bs + k\right)\left(K_1 + 2G + K_2\right)}{\left(3\tau^2 s^3 + 3\alpha\tau s^2 + \alpha\beta s\right)\left(\frac{1}{3}ms^2 + bs + k\right)} \tag{10}$$

where s denotes the Laplace variable, and α, β, and τ are the DMP parameters. G denotes the designed adaptive coupling term. Note that

$$K_1 = f_1 + \alpha\beta g_1 + O_1 \tag{11a}$$

$$K_2 = f_2 + \alpha\beta g_2 + O_2 \tag{11b}$$

where g_1, g_2 and f_1, f_2 are the goals and forces for the DMP trajectory X_1, X_2, respectively. By expanding Eq. (10), a form of generic polynomial expression can be derived as

$$X_p\left(s\right) = k_s\frac{Z_s\left(s\right)}{R_s\left(s\right)}, \tag{12}$$

where k_s is the high-frequency gain. R_s and Z_s are the Hurwitz polynomials, given by

$$R_s\left(s\right) = a_0 + a_1 s + \cdots + a_{n-1}s^{n-1} + s^n, \tag{13a}$$

$$Z_s\left(s\right) = b_0 + b_1 s + \cdots + b_{n-1}s^{m-1} + s^m, \tag{13b}$$

with degree n and m, respectively. Here, Eq. (10) is a high relative order system with a relative degree of $(n - m)$. The relatively high-order system can be approximated for the controller design by only keeping the low-frequency dominant poles. Hence, the original high relative degree system can be approximated by Eq. (14) with the relative degree system of $n - m = 1$ and then added by a scale factor C_b for equalizing the estimation system with the exact system:

$$X_p = \frac{C_b\left(bs\ +\ k\right)\left(K_1 + 2G + K_2\right)}{\frac{1}{3}ms^2 + bs + k}. \tag{14}$$

Based on Eq. (14), a multiple-input-single-output system is constructed. However, only the control input term G is controllable among the total three inputs K_1, K_2, and G. The two other inputs K_1 and K_2 are set at the initial instant t_0 or excited by the canonical system represented by Eq. (6). Moreover, the higher-order dynamics that are not included in the model can be solved in the application by the dead zone to prevent the problem of parameter drifting.

C. Controller Design and Convergence Analysis

In order to drive the plant signal X_p to track the desired reference signal and adaptively apply to the deformable object, the control input, which consists of the feedback and feedforward signal, the feedback gain matrix, and the feedforward gain can be designed as below

$$G = K(t)\, r + F(t)\, X_P, \tag{15}$$

$$K(t) = K(0) + \int_0^t \Gamma_2 \begin{bmatrix} B_m & \bar{K}^{-1} \end{bmatrix}^{\mathsf{T}} P e r^{\mathsf{T}} d\tau, \tag{16}$$

$$F(t) = F(0) + \int_0^t \Gamma_1 \begin{bmatrix} B_m & \bar{K}^{-1} \end{bmatrix}^{\mathsf{T}} P e X_p^{\mathsf{T}}\, d\tau, \tag{17}$$

where $K(t) \in \mathbb{R}^{m\times m}$ and $F(t) \in \mathbb{R}^{m\times n}$. Substituting the control input Eq. (15) into the plant dynamics of Eq. (1) yields the closed-loop system:

$$\dot{X}_p = (A_p + B_p F) X_P + B_p K r. \tag{18}$$

Here, the system out error is defined by $e = X_p - X_m$. Based on Eqs. (2) and (18), the error dynamics can be derived as

$$\dot{e} = A_m e + (A_m - A_p - B_p\ F) X_p + (B_m - B_p K) r. \tag{19}$$

In an ideal situation, the last two terms on the RHS of (19) should be equal to zero, and the optimal values of F and K should be rewritten as $\bar{F}$ and $\bar{K}$, respectively. Therefore, under the constraint of $|K| \neq 0$, we have

$$A_p = A_m - B_p \bar{F}, \tag{20a}$$

$$B_p = B_m \bar{K}^{-1}. \tag{20b}$$

On the basis of Eqs. (2) and (19), the error dynamics can be reformulated as

$$\dot{e} = A_m e + B_m \bar{K}^{-1} \phi X_p + B_m \bar{K}^{-1} \psi r, \tag{21}$$

where $\phi = \left(\bar{F} - F\right) \in \mathbb{R}^{m\times n}$ and $\psi = \left(\bar{K} - K\right) \in \mathbb{R}^{m\times m}$. Note that ϕ and ψ are the adjustable parameters.

The Lyapunov theory is utilized to prove the global stability of the designed system based on the designed control laws in Eq. (15) and the controller update laws in Eqs. (16) and (17).

Proof. First, in the augmented space that consists of tracking error e and adjustable parameter ϕ and ψ, the Lyapunov candidate function can be defined as

$$V = \frac{1}{2}\left[e^{\mathsf{T}} P e + \mathrm{Tr}\left(\phi^{\mathsf{T}} \Gamma_1^{-1} \phi + \psi^{\mathsf{T}} \Gamma_2^{-1} \psi\right)\right], \tag{22}$$

where P, Γ_1^{-1}, and Γ_2^{-1} are the positive definite matrices, and $\mathrm{Tr}(\cdot)$ denotes the matrix trace operator. Then, taking the derivative of Eq. (22) yields

$$\begin{aligned} \dot{V} =& \frac{1}{2}\Big[e^{\mathsf{T}} P \dot{e} + \dot{e}^{T} P e + \mathrm{Tr}\Big(\dot{\phi}^{\mathsf{T}} \Gamma_1^{-1} \phi + \phi^{\mathsf{T}} \Gamma_1^{-1} \dot{\phi} \\ & + \dot{\psi}^{\mathsf{T}} \Gamma_2^{-1} \psi + \psi^{\mathsf{T}} \Gamma_2^{-1} \dot{\psi}\Big)\Big]. \end{aligned} \tag{23}$$

Finally, substituting $\dot{e}$ into Eq. (23), one can get

$$\begin{aligned} \dot{V} =& \frac{1}{2} e^{\mathsf{T}} \left(P A_m + A_{mP}^{\mathsf{T}}\right) e \\ & + e^{\mathsf{T}} P B_m \bar{K}^{-1} \phi X_p + e^{\mathsf{T}} P B_m \bar{K}^{-1} \psi r \\ & + \frac{1}{2} \mathrm{Tr}\left(\dot{\phi}^{\mathsf{T}} \Gamma_1^{-1} \phi + \phi^{\mathsf{T}} \Gamma_1^{-1} \dot{\phi} + \dot{\psi}^{\mathsf{T}} \Gamma_2^{-1} \psi + \psi^{\mathsf{T}} \Gamma_2^{-1} \dot{\psi}\right). \end{aligned} \tag{24}$$

In Eq. (24), the second term $\left(e^{\mathsf{T}} P B_m \bar{K}^{-1} \phi\right) \in \mathbb{R}^{1\times n}$ and the third term $\left(e^{\mathsf{T}} P B_m \bar{K}^{-1} \psi\right) \in \mathbb{R}^{1\times m}$, therefore,

$$e^{\mathsf{T}} P B_m \bar{K}^{-1} \phi X_p = \mathrm{Tr}\left(X_p e^{\mathsf{T}} P B_m \bar{K}^{-1} \phi\right), \tag{25a}$$

$$e^{\mathsf{T}} P B_m \bar{K}^{-1} \psi r = \mathrm{Tr}\left(r e^{\mathsf{T}} P B_m \bar{K}^{-1} \psi\right), \tag{25b}$$

$$\mathrm{Tr}\left(\dot{\phi}^{\mathsf{T}} \Gamma_1^{-1} \phi\right) = \mathrm{Tr}\left(\phi^{\mathsf{T}} \Gamma_1^{-1} \dot{\phi}\right), \tag{25c}$$

$$\mathrm{Tr}\left(\dot{\psi}^{\mathsf{T}} \Gamma_1^{-1} \psi\right) = \mathrm{Tr}\left(\psi^{\mathsf{T}} \Gamma_1^{-1} \dot{\psi}\right), \tag{25d}$$

such that the original Eq. (23) can be reformulated as

$$\begin{aligned} \dot{V} =& \frac{1}{2} e^{\mathsf{T}} \left(P A_m + A_m^{\mathsf{T}} P\right) e \\ & + \mathrm{Tr}\left(\dot{\phi}^{\mathsf{T}} \Gamma_1^{-1} \phi + X_p e^{\mathsf{T}} P B_m \bar{K}^{-1} \phi\right) \\ & + \mathrm{Tr}\left(\dot{\psi}^{\mathsf{T}} \Gamma_2^{-1} \psi + r e^{\mathsf{T}} P B_m \bar{K}^{-1} \psi\right). \end{aligned} \tag{26}$$

Given that A_m is a stable matrix, the symmetric positive definite matrix Q can be chosen to satisfy the condition of $P A_m + A_m^{\mathsf{T}} P = -Q$. For $\forall e$ and $e \neq 0$, the first term in Eq. (26) is negative definite.

Here, we assumed that A_p or B_p are either constants or slowly change over time, which would result in $\dot{\bar{F}} \approx 0$ and $\dot{\bar{K}} \approx 0$. Also, the controller parameters update laws are given in Eq. (16) and (17). Hence, $\dot{F}$ and $\dot{K}$ can be updated as

$$\dot{F} = \dot{\bar{F}} - \dot{\phi} = \Gamma_1 \begin{bmatrix} B_m & \bar{K}^{-1} \end{bmatrix}^{\mathsf{T}} P e X_p^{\mathsf{T}} \tag{27}$$

$$\dot{K} = \dot{\bar{K}} - \dot{\psi} = \Gamma_2 \begin{bmatrix} B_m & \bar{K}^{-1} \end{bmatrix}^{\mathsf{T}} P e r^{\mathsf{T}}. \tag{28}$$

Then, the update rate of the parameters error can be computed as

$$\dot{\phi} = -\Gamma_1 \begin{bmatrix} B_m & \bar{K}^{-1} \end{bmatrix}^{\mathsf{T}} P e X_p^{\mathsf{T}} \tag{29}$$

$$\dot{\psi} = -\Gamma_2 \begin{bmatrix} B_m & \bar{K}^{-1} \end{bmatrix}^{\mathsf{T}} P e r^{\mathsf{T}}. \tag{30}$$

Substituting the Eqs. (29) and (30) into Eq. (26), the last two terms on the RHS can be canceled out and $\dot{V}$ in Eq. (23) can be guaranteed as a negative definite matrix. Error dynamics e can be guaranteed to asymptotically converge with $\lim_{t\to\infty} e(t) = 0$. The control diagram of the system is given in Fig. 3. ∎

IV. Simulation Trials

To validate the proposed approach, we performed extensive simulations to evaluate the manipulation accuracy and the adaptiveness that withstands the uncertainty caused by plant model parameters. These simulation experiments aim to transport the grabbed deformable object to the desired goal position along with the DMP generalized path. Notably, two robot manipulators transport the grabbed deformable objects, imitating different demonstrated trajectories while facing several obstacles. The simulations were implemented in the C++ version of the open-source Bullet physics library[1]. Also, Matlab Simulink environment is deployed to test the semi-ellipse trajectory and three obstacles case in Table I. Readers may also refer to our repository[2] to test our algorithm.

[1]Bullet Physics Library: https://github.com/bulletphysics/bullet3

[2]Matlab code: https://github.com/cuizhenxi8/RALMatlab

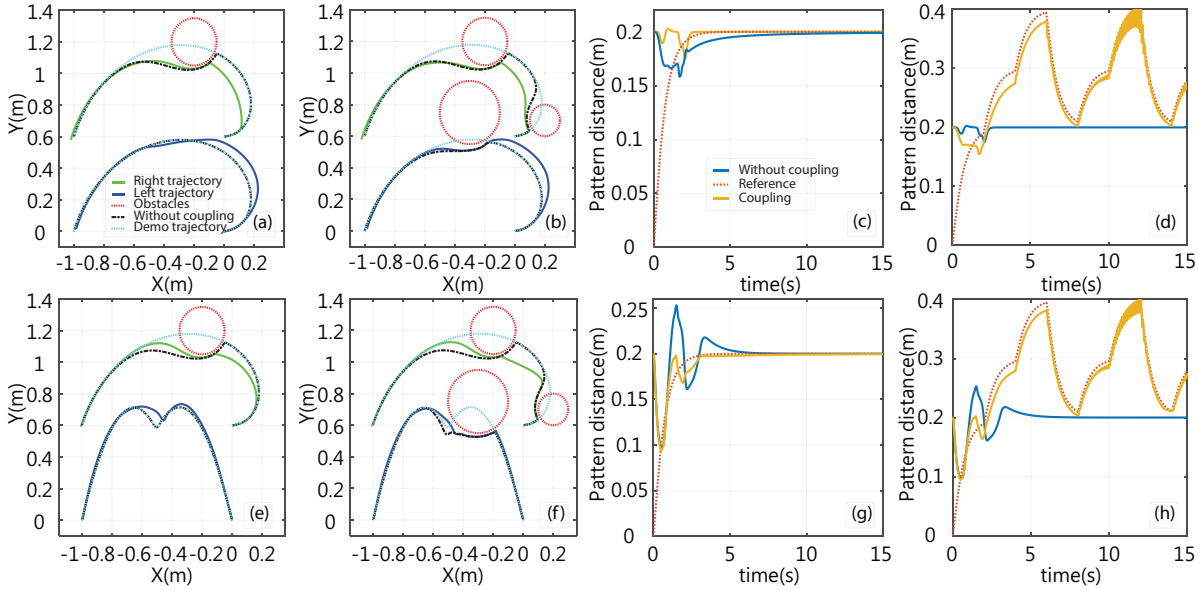

Figure 4. DMP generalization on semi-ellipse shape (a)–(d) and 'M' shape trajectories (e)–(h). Results of single (a, e) and multiple (b, f) obstacles intruded along the trajectories. Two different selection of a constant reference signal (c, g) $r = 0.2$ and a gradually changing signal (d, h) $r = [0.2, 0.3, 0.4]$ are separately tested.

Table I
CONFIGURATION OF THE EXPERIMENTS[a]

		Semi-ellipse trajectory		M-shape trajectory	
		Start	Goal	Start	Goal
Pattern/ Grabbing Points	X_3	(0, 0)	(-1, 0)	(0, 0)	(-1, 0)
	X_1	(0, 0.2)	(-1, 0.2)	(0, 0.2)	(-1, 0.2)
	X_2	(0, 0.4)	(-1, 0.4)	(0, 0.4)	(-1, 0.4)
	X_4	(0, 0.6)	(-1, 0.6)	(0, 0.6)	(-1, 0.6)
Number of Obstacles	1	(-0.2, 1.2, 0.15, 0.15)		(-0.2, 1.2, 0.15, 0.15)	
	3	(-0.2, 1.2, 0.15, 0.15) (0.2, 0.7, 0.1, 0.1) (0.3, 0.75, 0.2, 0.2)		(-0.2, 1.2, 0.15, 0.15) (0.2, 0.7, 0.1, 0.1) (0.3, 0.75, 0.2, 0.2)	

[a]Coordinate Unit Length are all in Metres.

A. *Simulation of Coupled DMP transportation in 2D*

1) ***The Same Demonstrated Trajectory for Two Arms Coupled DMP Generalization****:* In this group of experiments, we manually demonstrated the semi-ellipse trajectory for both manipulators. Although simple, many types of human-like behavior can be represented by this trajectory, such as folding cloth and objects were fetching over the obstacle. The starting and goal coordinated of points X_3, X_1, X_2 and X_4 in different experiment configurations are shown in Table I.

According to Fig. 4(a), the cyan dotted lines in the form of semi-ellipse are the demonstrated trajectory for the left and right manipulators. The red dotted line represents the obstacle that must be avoided. Based on the proposed method, the solid blue and green lines are the actual left and right DMP generalization. For comparison, the black line shows the manipulator DMP trajectory without utilizing the proposed coupling term, where the DMP independently generalizes the new trajectory based on the start, goal, and the demonstrated trajectory. Fig. 4(a) illustrates that the left and right DMP can generalize the trajectory based on the demonstrated semi-ellipse from the start point to the goal point.

Moreover, while the right DMP successfully avoids the obstacle, the obstacle avoidance action is transported to the opposite coupled DMP utilizing our proposed method. The difference between the coupled generalized DMP trajectory(solid green and blue lines) and the uncoupled DMP trajectory (dotted black line) can illustrate the effects on the generalization of the coupled DMP. The left-side DMP accordingly shifts to the negative Y-axis when the right-side DMP attempts to avoid obstacles. In this way, the configuration of the deformable object can be preserved. It can be observed in Fig. 4(c) that the pattern's configuration, which is the distance between the two patterns, is gradually converged to the desired value of 0.2, even though a slight vibration when avoiding the collision at a time index of 2. To test the signal tracking ability, we gradually change the reference distance in a repeated manner of $[0.2, 0.3, 0.4]$ shown as the red dotted line in Fig. 4(d).

The overall tracking performance is satisfactory, where the detected output signal can track the reference signal. Furthermore, we tested the proposed method in the situation of multiple obstacles spread on both sides of the manipulators, as illustrated in Fig. 4(b). It can be noticed that both DMPs can adaptively generalize the desired DMP according to the demonstrated trajectory. Although the two-side obstacle gives additional requirements for the DMP generalization, the obstacles could be perfectly avoided.

2) ***Different Demonstrated Trajectories for Two Arms Coupled DMP Generalization****:* Apart from the same trajectory generalization (left and right side X_3 and X_4 learning the same semi-ellipse trajectory), we also tested the case where the left and right DMP imitated different demonstrated trajectories. Here, the demonstrated path for the right manipulator is the semi-ellipse, whereas the left manipulator is imitating an M-shape, which is shown in Fig. 4(e).

In the first situation of a single obstacle, the right and left

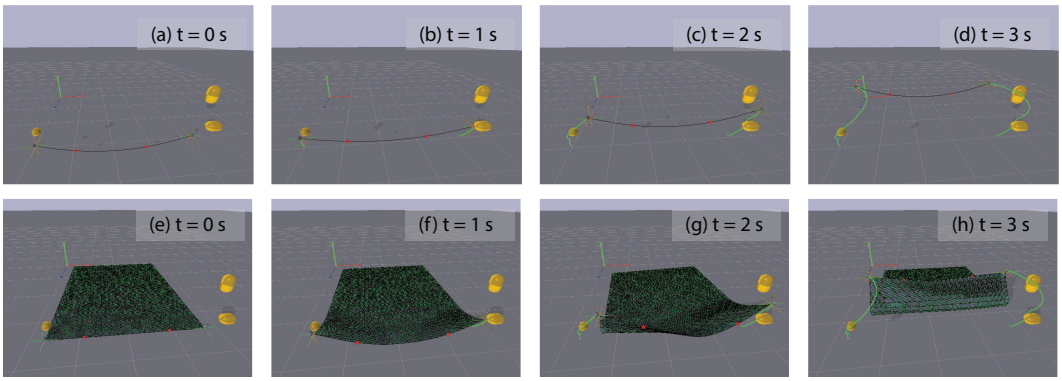

Figure 5. Cooperative transport of rope (a)-(d) and cloth (e)-(h) while maintaining red pattern dots distance constantly at $r = 0.2$ during transportation. The green solid line denotes the planned DMP trajectory. The black solid curve denotes the rope. The green thin film denotes the cloth. The yellow-colored shapes are obstacles in the environment.

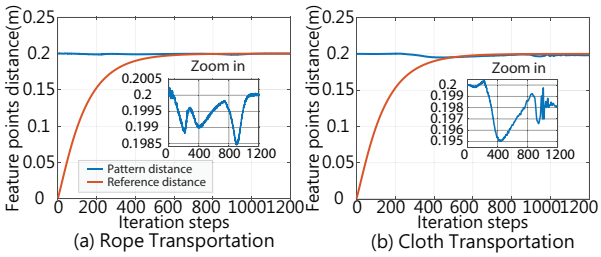

Figure 6. Constant pattern distance.

DMPs can generalize the desired trajectory according to the demonstrated trajectory. Because of the introduced coupled term, the left-side DMP can accordingly adjust when the right-side DMP faces an obstacle. Based on the proposed coupled term, the error of the configuration can converge into the desired level of 0.2, as shown in Fig. 4(g). Compared with the without coupling case, the proposed method generates less perturbation when the DMP tries to avoid the collision at the time index of 2. As a comparison, the without coupling scenario is tested and is shown as the black dotted line. A clear difference can be noticed between our method (green and blue line) and the without coupling method (black line), especially for the right-side DMP either in single or multi-obstacle cases. Here, the coupled term affects both sides to guarantee that the DMP can generalize to the goal position while avoiding the obstacles. To reach the goal position, both DMP sides can achieve this requirement, as shown in Fig. 4(e) and Fig. 4(f). During the manipulation, the pattern configuration error can slowly converge to the desired value of 0.2. Compared with the without coupling scenario, our method suffers a smaller fluctuation, which is desirable in stabilizing the pattern configuration perturbation. Moreover, the reference stair signal was tested, and the result is shown in Fig. 4(h). It can be noticed that the changing signal can be adequately traced even though the complexity of demonstrated trajectory is increased.

B. Simulation on Rope and Cloth Transportation in 3D

The following part assumes that the end-effector can perfectly track the designed DMP trajectory while the manipulated object is firmly grabbed. Also, the coordination of the end-effector and pattern points can be measured. Here, the task is to transport the grabbed rope and cloth from the initial position to the goal position imitating the prior demonstrated trajectory. The designed coupled DMP trajectory should preserve the desired pattern distance (constant or variable) as much as possible even under the uncertainty of the manipulated object model and the appearance of the obstacles on the path.

*1) **Constant Pattern Distance Transportation**:* In this experiment, the distance of the pattern represented by the red dots on the rope and cloth edge should preserve constant during the transportation. For the transportation task, both the rope and cloth can complete the deformable object transportation while mimicking the prior demonstrated trajectory as shown in Fig. 5(a)-(d). Slight disturbance can be observed during transportation. However, the disturbance scales for both cases are small, compared to the desired value of 0.2. Hence, the pattern disturbance can be roughly kept constant to complete the manipulation as shown in Fig. 6(a) and (b).

For the deformable cloth transportation, the manipulation is not as good as the rope transportation from the perspective of the maximum disturbance and the steady-state value as shown in Fig. 6(b). It is because the 2D deformable object suffers more from the relative dragging and self-collision effects, as shown in Fig. 5(f) and (g). This problem can be alleviated by increasing the gripper number according to the number of coupled DMP.

*2) **Variable Pattern Distance Transportation**:* The pattern distance needs to track a variable signal which is firstly decreased from 0.2 to 0.14 as shown in Fig. 7, then increase back to 0.2. There are many applications for this scenario, such as moving and transferring patients using bedsheets passing through the hospital corridor or room door [18]. The coupled DMP trajectory generalized from their demonstrated path first decreases and then increases along with the reference signal as shown in Fig. 8(a) and (b). Tracking errors can be observed during rope and cloth transportation manipulation. This error is related to the coefficient of Γ_1 and Γ_2 shown in equations (16) and (17). Increasing their values could decrease the tracking error in the manipulation. However, it could increase the probability of the downside overshoot problem. Hence, there is a trade-off in the parameter setting of Γ_1 and Γ_2. Their empirical values are set as 30 and 0.6 for the rope, while 1500

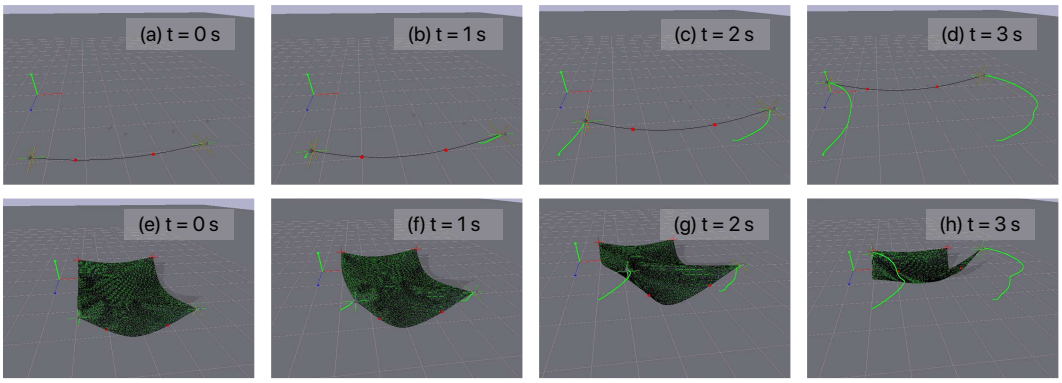

Figure 7. Collaborative transport of rope (a)-(d) and cloth (e)-(h) while maintaining red pattern dots distance variablely at $r = [0.14, 0.2]$ during transportation. The green solid line denotes the planned DMP trajectory. The black solid curve denotes the rope. The green thin film denotes the cloth. The yellow-colored shapes are obstacles in the environment.

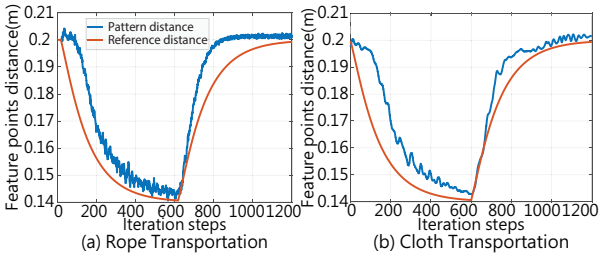

Figure 8. Variable pattern distance.

and 5 for the cloth. Even though disturbance can be observed as in the constant distance experiments, our method can track the overall reference signal properly.

V. Robotic Experiments

We further implemented the proposed method on a dual-UR3 platform with depth visual feedback for deformable object transportation. The robot grippers transported the grabbed object to mimic the demonstrated trajectory while limiting the Euclidean norm error of the markers. In this regard, two tennis balls were statically set as the avoidable obstacles along the path. Two kinds of deformable objects with different stiffness (bungee cord and cotton rope) were tested, and their modeling parameters are unknown to our model-based controller. The experiment performance between our coupling method and the uncoupled method was examined, with comparison provided.

The result of the first experiment on the bungee cord with two markers distance set at 16 cm is demonstrated in Fig. 9(a). The coupling and un-coupled methods can successfully transport the deformable object while mimicking the demonstrated trajectory and avoiding obstacles on the path. The marker distance in both methods slightly oscillates around 2 cm. Our method, however, suffers less error when the obstacles on the path as shown in iteration steps of 110 and 300. It is because that proposed controller listed in Eq. (15)–(17) can introduce the coupling control term into the engaged DMP trajectories so that the avoiding action can be transferred from one side to another side. Even though only one side is facing the obstacles, it can be noticed that both coupled DMP update accordingly to avoid the obstacles while minimizing the disruption to the deformable object. In this way, the norm distance of the markers can be preserved as desired, and multiple DMP can be coupled together. In contrast, the uncoupling method cannot synchronize two engaged DMP trajectories during the transportation task. As the coupling term is missing, each side DMP can only react to the obstacle appearing on their path. Hence, the transportation result is not as good as our method.

In the second experiment, we replaced the manipulated bungee cord with cotton rope with the markers' distance of 18 cm to test our method on low stiffness objects. Based on the result in Fig. 9, we can notice that the maximum magnitude error for the case of cotton rope reduces from 2 cm to 1.5 cm, compared with that of the bungee cord. The cotton rope suffers less fluctuation during the manipulation than the bungee cord cases. At a small range of iteration steps (250 to 350), our coupled method seems to suffer more significant error than the uncoupled method, which may be caused by the measurement noise of the depth camera. However, the error fluctuation based on our method is smaller than the uncoupled methods, which is an advantage in some precision tasks.

Although the proposed algorithm was validated through simulation and experiments, some observations and limitations are also noted. In the experiment, mild oscillation or divergence in some phases can be observed, especially when the robot arm passes through obstacles. The reason is that, on the one hand, in terms of the model implementation, the high order parts of the plant model are omitted in Eq. (14) to match the low order reference model for the sake of simplicity of the controller design. On the other hand, the measurement noise is not fully considered in the proposed controller design. All the above factors may cause the reference model Eq. (3) to match with the simplified model but cannot conform to the deformable object model.

VI. Conclusions

This study proposes a dynamically coupled multiple DMP generalization method for the dual-arm manipulation of deformable objects. To solve the uncertainty from the model parameters of deformable objects, we propose using the reference model to introduce the coupling term into the multiple DMP generalization adaptively. On this basis, the proposed method can adaptively estimate the undetermined model parameters, which can widen possible applications, such as deformable

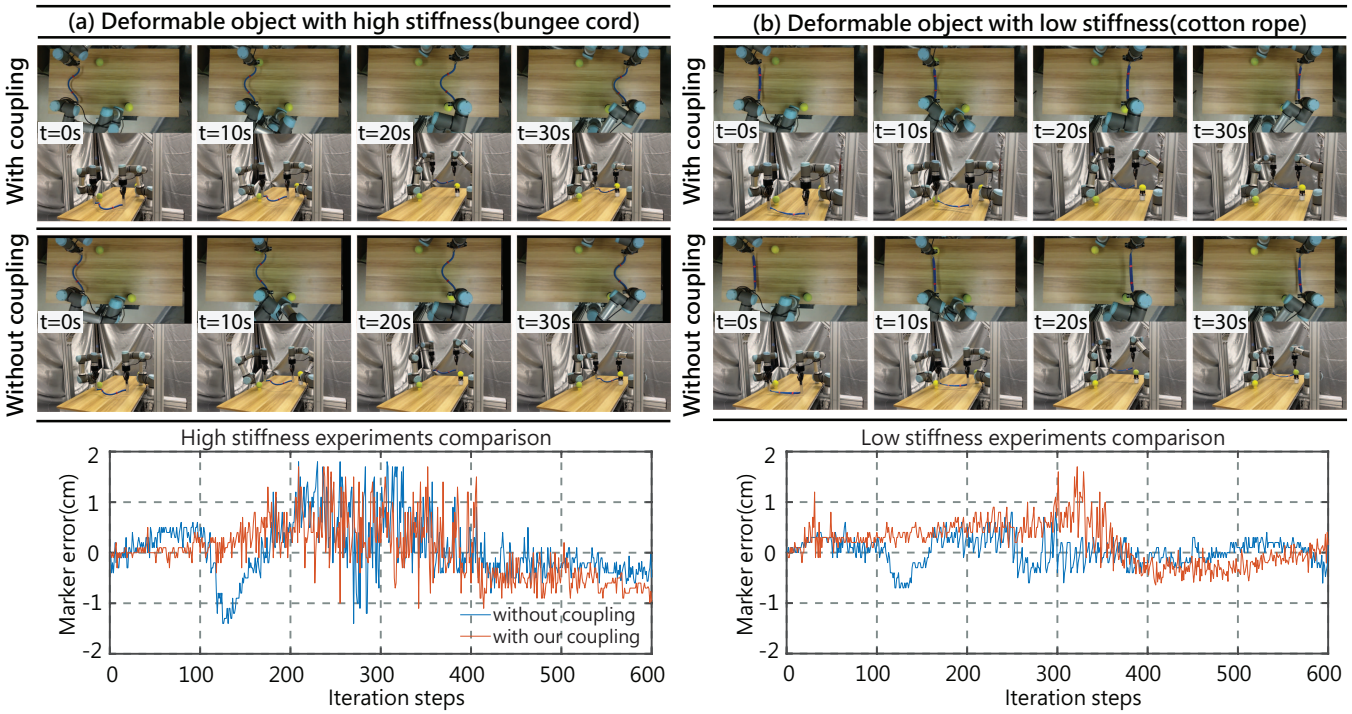

Figure 9. The coupled DMP transportation for 60 cm from the initial to goal position while preserving the markers norm distance at (a) 16 cm and in (b) 18 cm. The measured markers norm errors are given below the snapshots.

rope and thin-film transportation. The DMP generalization, pattern configuration preserving, and collision avoidance are compactly modeled in one integrated second-order system, making the system flexible for implementation and maintenance in real-world applications. Extensive simulations were performed on the open-source physical platform to validate our method without losing generality. We also implemented our method on a dual-arm robot platform to further support the method's applicability.

In the future, preserving complex configurations formed by feature points' distance and orientation would be worth exploring. Benefiting from the DMP intrinsic canonical system in Eq. (6) and our proposed control framework, temporal coupling across multiple degrees of freedom can be researched where multi-agent cooperative object manipulation can be realized more conveniently. Also, the contact force between the manipulator and the manipulated object could be included to make the whole control system more adaptive and robust.

References

[1] S. Schaal, "Dynamic movement primitives-a framework for motor control in humans and humanoid robotics," in *Adaptive motion of animals and machines*. Springer, 2006, pp. 261–280.

[2] F. Stulp *et al.*, "Reinforcement learning with sequences of motion primitives for robust manipulation," *IEEE Trans. Robot.*, vol. 28, no. 6, pp. 1360–1370, 2012.

[3] M. Tamosiunaite *et al.*, "Learning to pour with a robot arm combining goal and shape learning for dynamic movement primitives," *Robot. Auton. Syst.*, vol. 59, no. 11, pp. 910–922, 2011.

[4] A. Paraschos *et al.*, "Probabilistic prioritization of movement primitives," *IEEE Robot. Autom. Lett.*, vol. 2, no. 4, pp. 2294–2301, 2017.

[5] M. Ginesi *et al.*, "Dynamic movement primitives: Volumetric obstacle avoidance," in *Int. Conf. Adv. Robot. (ICAR)*, 2019, pp. 234–239.

[6] H. Kim *et al.*, "Incorporating safety into parametric dynamic movement primitives," *IEEE Robot. Autom. Lett.*, vol. 4, no. 3, pp. 2260–2267, 2019.

[7] A. Dahlin and Y. Karayiannidis, "Temporal coupling of dynamical movement primitives for constrained velocities and accelerations," *IEEE Robot. Autom. Lett.*, vol. 6, no. 2, pp. 2233–2239, 2021.

[8] T. Kulvicius *et al.*, "Interaction learning for dynamic movement primitives used in cooperative robotic tasks," *Robot. Auton. Syst.*, vol. 61, no. 12, pp. 1450–1459, 2013.

[9] A. Gams *et al.*, "Coupling movement primitives: Interaction with the environment and bimanual tasks," *IEEE Trans. Robot.*, vol. 30, no. 4, pp. 816–830, 2014.

[10] B. Nemec *et al.*, "Bimanual human robot cooperation with adaptive stiffness control," in *IEEE/RAS 16th Int. Conf. Humanoid Robot. (Humanoids)*, 2016, pp. 607–613.

[11] B. Nemec *et al.*, "Human robot cooperation with compliance adaptation along the motion trajectory," *Auton. Robot.*, vol. 42, no. 5, pp. 1023–1035, 2018.

[12] Y. Zhou *et al.*, "Coordinate change dynamic movement primitives—a leader-follower approach," in *IEEE/RSJ Int. Conf. Intell. Robot. Syst. (IROS)*, 2016, pp. 5481–5488.

[13] H. B. Amor *et al.*, "Interaction primitives for human-robot cooperation tasks," in *IEEE Int. Conf. Robot. Autom. (ICRA)*, 2014, pp. 2831–2837.

[14] G. Sun *et al.*, "Adaptive vision-based control for rope-climbing robot manipulator," in *IEEE/RSJ Int. Conf. Intell. Robot. Syst. (IROS)*, 2019, pp. 1454–1459.

[15] M. Meyer *et al.*, "Interactive animation of cloth-like objects in virtual reality," *J. Vis. Comput. Animat.*, vol. 12, no. 1, pp. 1–12, 2001.

[16] A. J. Ijspeert *et al.*, "Movement imitation with nonlinear dynamical systems in humanoid robots," in *IEEE Int. Conf. Robot. Autom. (ICRA)*, vol. 2, 2002, pp. 1398–1403.

[17] D.-H. Park *et al.*, "Movement reproduction and obstacle avoidance with dynamic movement primitives and potential fields," in *IEEE/RAS 8th Int. Conf. Humanoid Robot. (Humanoids)*, 2008, pp. 91–98.

[18] B. Roy *et al.*, "Repositioning of a rigid body with a flexible sheet and its application to an automated rehabilitation bed," *IEEE Trans. Autom. Sci. Eng.*, vol. 2, no. 3, pp. 300–307, 2005.